Higher Temperatures Yield Smaller Grains in a Thermally Stable Phase-Transforming Nanocrystalline Alloy

Dor Amram* and Christopher A. Schuh
Department of Materials Science and Engineering, Massachusetts Institute of Technology, 77 Massachusetts Avenue, Cambridge, Massachusetts 02139, USA

(Received 15 August 2018; published 1 October 2018)

Grains in crystalline materials usually grow with increased thermal exposure. Classical phenomena such as recrystallization may lead to a purely temporary decrease in the grain size, while recent advances in alloy design can yield thermally stable nanocrystalline materials in which grain growth stagnates. But grains never shrink, since there is a lack of interface-generating mechanisms at high temperatures, which are required to decrease the grain size if such was the system's thermodynamic tendency. Here we sidestep this paradigm by designing a nanocrystalline alloy having an allotropic phase transformation—an interface-generating mechanism—such that only the high-temperature phase is stabilized against grain growth. We demonstrate that for an Fe-Au alloy cycled through the $\alpha \leftrightarrow \gamma$ transformation, the high-temperature phase (γ-Fe) has a stable fine grain size, smaller than its low-temperature counterpart (α-Fe). The result is an unusual material in which an increase in temperature leads to finer grains that are stable in size.

DOI: 10.1103/PhysRevLett.121.145503

One of the most common themes in materials science, grain growth is ubiquitous in nature [1,2]. In crystalline materials, it stems from the inherent energetic penalty that drives the material to eliminate grain boundaries, en route to a thermodynamically favored single crystal [3]. One feature of grain growth is that it is monotonic, ever increasing with time at temperature, although the details of the time and temperature dependencies can vary and be quite complex [4–6]. Very few significant deviations from monotonic grain growth are known, for which two primary families of phenomena can be held accountable, as illustrated in Fig. 1. The first involves recrystallization in response to large amounts of stored defect energy, often introduced by plastic deformation [7], or in response to a phase transformation as, for example, in austenitizing of steel [8]. Similarly, some solid-state reactions, such as discontinuous precipitation, may also result in transient grain refinement due to vacancy supersaturation, though the magnitude of this effect is typically small [9]. Such cases allow for the formation of many new fine grains, which effectively reduces the average grain size upon annealing. However, once this excess energy is released, the system proceeds to conventional grain growth; the initial grain shrinkage is only transient in nature. The second deviatory phenomenon is grain size stabilization or the arrest of grain growth once grains have reached a certain size [10]. Such a stable grain size can be dictated by kinetic impediments, such as second phase precipitates [11,12] or grain boundary grooving and other surface-related phenomena in thin films [13–15]. More recently, in alloyed nanocrystalline materials, grain size stabilization has become associated with thermodynamic considerations (grain boundary segregation) [10,16,17]. Regardless of stabilization mechanism, thermally stable grain structures reach their stable grain size "from below": their initial grain structure is commonly obtained by some nonequilibrium processing method and is finer than the stable size to which the system grows [18] (Fig. 1).

We are not aware of cases where a stable grain size is approached "from above," i.e., occurring by a natural

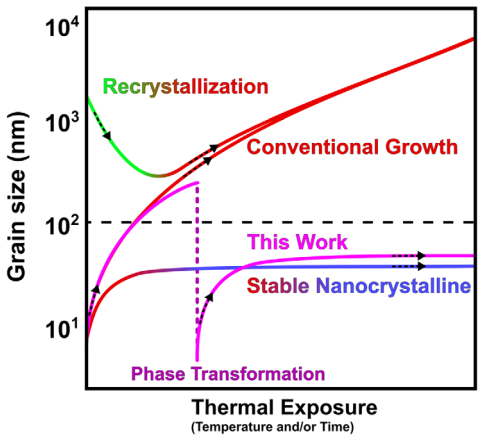

FIG. 1. Grain growth. Schematic illustration of grain growth in materials (grain size as a function of exposure to temperature and/or time), identifying several distinct behaviors shown by the different curves. Colors indicate growth (red), shrinkage (green), and stability (blue), and arrows accompany these trends. The unique behavior observed in this work (magenta) is an effective reduction and stabilization of the grain size after a phase transformation.

mechanism of grain shrinkage. Theoretically, in alloyed systems involving grain boundary segregation there is support for such grain shrinkage being energetically plausible, as a finer grain size can accommodate more solute segregation and can therefore offset an energy penalty of dissolving that solute in the grains [19]. However, spontaneous grain shrinkage would require an interface-generating mechanism to increase the total grain boundary area (i.e., reduce the grain size).

In this Letter, we propose a method to sidestep the monotonic grain growth paradigm by combining the two "deviating" phenomena above. By combining a recrystallizationlike event to produce additional grain boundary area, with a segregation-based stabilization mechanism, we report an alloy designed to exhibit grains that shrink and remain fine in a stable condition following a high-temperature phase transformation. In such an alloy, we expect the grains of the high-temperature phase to be stable and smaller compared with its low-temperature counterpart, so that the grain size is effectively reduced even though the temperature increased, as illustrated in Fig. 1.

To demonstrate this behavior, we begin our alloy design process with the regular nanocrystalline solution model [20] and subsequent improvements of it [21–23]. The output of this model is a "stability map," which is divided into three distinct zones [22]. Each map is plotted for a particular solvent and is populated by solutes based on their bulk enthalpy (comprised of the enthalpy of mixing ΔH_{mix} and enthalpy of compound formation ΔH_c) and the enthalpy of grain boundary segregation ΔH_{seg} (see Fig. 2). A desired microstructure can then be designed by the appropriate choice of solute. Here we retain the simplicity of a binary

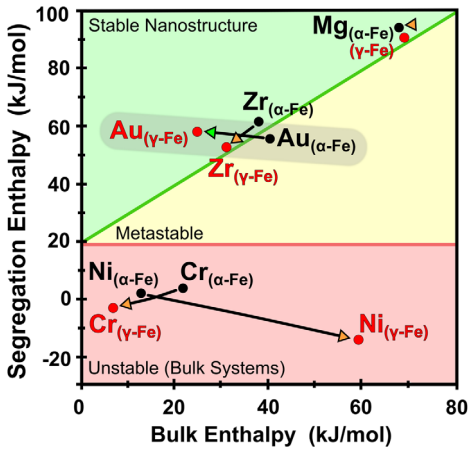

FIG. 2. Nanocrystalline stability map. A map of enthalpy of grain boundary segregation vs bulk enthalpy (defined in a previous work [22] and in the Supplemental Material [24]) for different solutes in Fe. Lines and colors identify three distinct zones, which are labeled. Several solutes populate the map with data for both α-Fe (in black) and γ-Fe (in red). Arrows indicate the change in the solutes position on the map upon the $\alpha \rightarrow \gamma$ transformation.

alloy but consider the inclusion of different structural phases (allotropes) of a solvent in the construction of the stability map. The rationale behind this choice is that these transformations generate interfaces spontaneously at elevated temperatures [3]: grains of the new phase grow from atomically small nuclei and therefore have a fair chance to find their equilibrium grain size during their transformation out of the parent phase. The details of our model are provided in the Supplemental Material [24]. To the best of our knowledge, the inclusion of an allotropic phase transformation in the design of nanocrystalline alloys has not been considered before, and very few works have explored such transformations in the nanocrystalline framework. In those works, Kotan *et al.* [45] and Huang *et al.* [46] studied the thermal stability of ball-milled $Fe_{91}Ni_8Zr$ alloys at different temperatures and found that the high-temperature phase (γ-Fe) had a notably higher grain size than its low-temperature counterpart (α-Fe). Note that this is consistent with conventional expectations for monotonic grain growth, with higher temperatures leading to larger grains. We return to analyze and compare our results with these in a subsequent section.

In the context of the map in Fig. 2, upon a phase transformation, a solute may cross a stability line into a different stability zone, thereby altering the thermodynamically favored microstructure of the material. We are particularly interested in the case where this occurs between a coarse-grained or bulk state (red and yellow zones in Fig. 2) to a stable nanocrystalline state (green zone in Fig. 2). Under such circumstances, the low-temperature phase may exhibit coarsening of its grains, whereas the high-temperature phase may adopt a stable nanocrystalline state. Upon heating across the transformation temperature, such an alloy would exhibit the desired deviatory behavior from monotonic grain growth, in which the grain size would shrink upon the transformation event and then remain stable at the nanoscale. To find such a system, we populate the stability map for Fe in Fig. 2 with several metallic solutes that were recently used in nanocrystalline Fe-based alloys [45–49]: Zr, Ni, Mg, Cr, and Au. Upon the $\alpha \rightarrow \gamma$ transformation, most solutes shift their position on this map, but remain within the same stability zone. However, Au presents a notable exception because in α-Fe it favors bulk phase structures, while in the high-temperature phase γ-Fe, its position in the map moves into the "nanostructure" zone. Therefore, Fe-Au alloys are promising candidates for the proposed deviatory grain growth behavior we seek.

We prepared nanocrystalline $Fe_{95}Au_5$ powders by high-energy ball milling of elemental powders. The milling process results in micron-sized powders composed of a homogeneous α-Fe solid solution supersaturated with Au, with a grain size of about 10 nm, similar to other nanocrystalline alloys prepared by this route [48]. We then performed *in situ* x-ray diffraction (XRD) experiments at elevated temperatures to study the microstructure evolution

and phase transformation in the powders as a function of time and temperature (see Supplemental Material [24] for complete experimental details). Figure 3(a) shows the Fe grain size during annealing. First, the grain size of α-Fe is shown at 700 and 800 °C, growing over 2.5 h at each temperature. Upon heating to 1000 °C γ-Fe is produced through the allotropic transformation (which is completed by the start of the measurement), and its grain size stabilizes quickly at that temperature and at 1100 °C as well. The most striking feature in Fig. 3(a) is that the grain size of γ-Fe at 1000 °C stabilizes at a smaller value (~115 nm) than the grain size of its parent phase α-Fe (~130 nm) at the substantially lower temperature of 800 °C. Even at 1100 °C (nearly 80% of the alloy's absolute melting temperature), the grain size of γ-Fe stabilizes rapidly at ~130 nm.

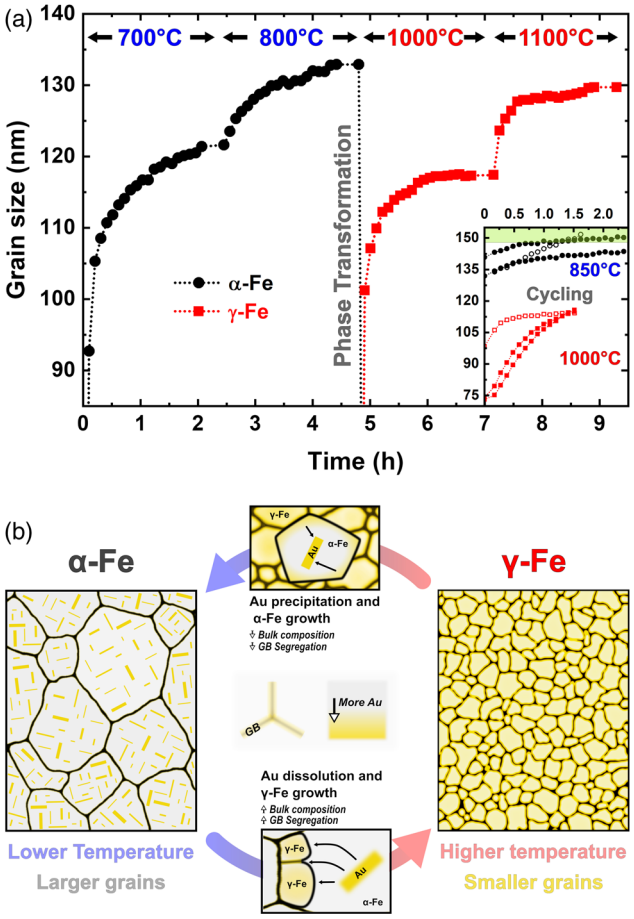

FIG. 3. *In situ* grain growth and phase transformation in nanocrystalline $Fe_{95}Au_5$. (a) Grain size as a function of time for α-Fe (at 700 and 800 °C) and for γ-Fe (at 1000 and 1100 °C). The inset shows the grain size after several cycles between 850 and 1000 °C. These curves are shifted to have a common time origin, and the first cycle is marked by open symbols. The resolution limit is marked in green. (b) Schematic illustration of α-Fe microstructure with Au nanoprecipitates and its transformation into γ-Fe. Both schematics are at the same scale and the suggested transformation mechanism is shown.

The results in Fig. 3(a) reflect the prediction of the stability map in Fig. 2: upon the allotropic transformation, Au shifts to the nanostructure zone in the γ-Fe phase and follows Fig. 1—grain growth following the phase transformation arrests at a lower value than prior to it.

To better understand this result, we conducted an additional *in situ* XRD experiment where the powder was cycled through the transformation several times, with the essential features shown in the inset of Fig. 3(a). There, three cycles through the transformation (at 850 and 1000 °C) are shown. The grain growth curves are shifted on the time axis to have a common origin and exhibit the same behavior: the grain size of γ-Fe is always lower than that of α-Fe. This is unique since, after the first cycle, the heavily deformed ball-milled microstructure is essentially erased, so that this effect is shown on a "clean slate." Indeed, the first cycle in the inset of Fig. 3(a) appears slightly different from the others. The cycling procedure is shown in full detail in Fig. S1, where the precipitation and dissolution of Au were also tracked: Au clearly precipitates out of α-Fe and grows with time, but is then completely dissolved in γ-Fe. This behavior also recurs with subsequent cycling.

Since the Fe $\alpha \leftrightarrow \gamma$ transformation mechanism has been the subject of countless works, we do not focus on it here. Instead, we provide a simple schematic illustration of microstructure evolution during and after the transformation in Fig. 3(b), which depicts our view of the transformation based on the XRD results and the known morphology of phase transformations in the Fe-Au system. The legend in the center of Fig. 3(b) depicts increasing Au content based on color (gray to gold), as well as grain boundary (GB) segregation. The microstructure of α-Fe is shown on the left: Fe-rich grains contain dissolved Au at the solubility limit. The remaining Au can be found in elongated nanoprecipitates; their morphology is based on TEM shown in Fig. S2 and is described in the Supplemental Material [24]. Upon heating past the transformation temperature, these dissolve and Au diffuses into newly forming γ-Fe grains, which nucleate at α-Fe grain boundaries and triple lines. These γ-Fe grains grow, reaching a smaller size than their parent grains, resulting in a finer microstructure in which Au is completely dissolved and, importantly, decorates the grain boundaries, providing stability to the grain structure. Upon cooling, the reverse transformation occurs and α-Fe grains grow as Au precipitates from solution, forming the nanoprecipitates. The grains continue to grow with time, resulting in a coarser microstructure than before.

We compare our results to a set of different nanocrystalline alloys prepared, annealed, and characterized in the exact same manner as our Fe-Au powders: pure Fe, $Fe_{85}Mg_{15}$, $Fe_{81}Cr_{19}Mg$, and $Fe_{90}B_{10}$. We also compare with the two prior published works on grain growth and phase transformation in nanocrystalline alloys: those of Kotan *et al.* [45]

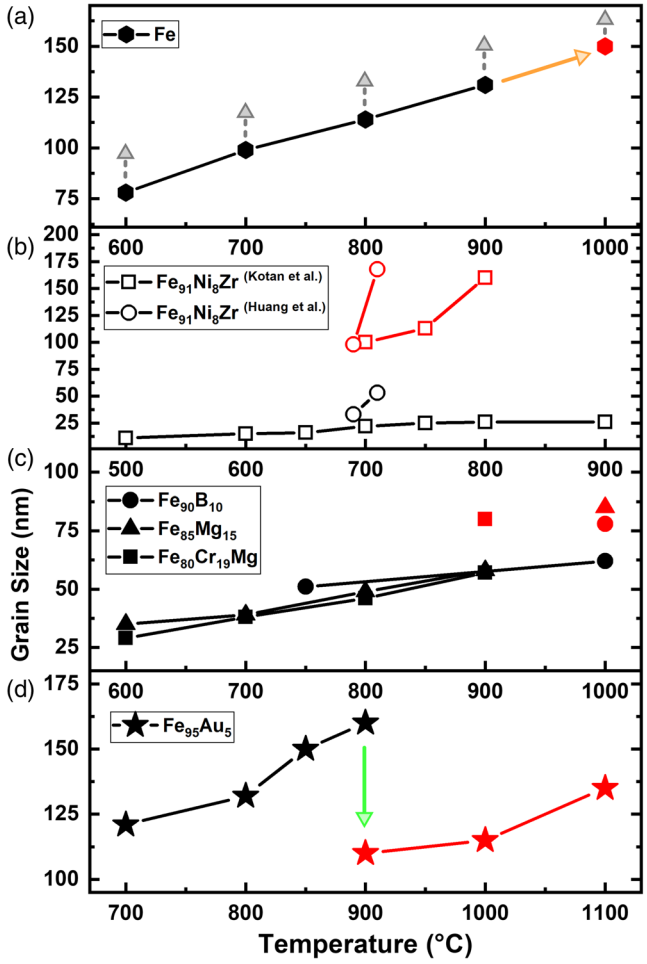

FIG. 4. Grain growth in different nanocrystalline alloys. A compilation and comparison of grain sizes in different nanocrystalline alloys as a function of annealing temperature through the transformation, from this work (a)–(d) and the literature (b). Only the Fe-Au alloy exhibits a decrease in grain size after the transformation. Black and red labels represent data for apparently stable grain size α- and γ-Fe, respectively, and open symbols denote literature data, for which stabilization of the grain size was expected, but not verified. Data for pure Fe (a) are accompanied by upward-pointing arrows to indicate a metastable grain size, which is expected to grow with increasing annealing time at each temperature.

and Huang *et al.* [46] on $Fe_{91}Ni_8Zr$. The comparison is shown in Fig. 4, where the grain size is plotted as a function of annealing temperature for both phases. Our results [Figs. 4(c) and 4(d)] represent the apparently stable grain size at each temperature, i.e., the saturation grain size that appears to be unchanging at the end of an annealing time of 2–3 h per temperature; in literature results [Fig. 4(b)], the annealing time was much shorter and grain size stability was not reported, although is principally expected for Zr (Fig. 2). As a baseline, we examined the grain size of pure nanocrystalline Fe through the phase transformation [Fig. 4(a)]: the grain size increased with temperature through the transformation. The data points are accompanied by upward-pointing arrows to indicate metastability, meaning that grains would continue to coarsen if the annealing time at each temperature (which was consistent between all of our experiments) was longer. Regardless, the grain size of γ-Fe is expectedly higher than that of α-Fe. This trend repeats for all other alloys and is especially pronounced in the results for $Fe_{91}Ni_8Zr$ alloys. These results are in line with the stability map shown in Fig. 2: stabilizing alloying elements, such as Mg and Zr, lend substantial thermal stability to α-Fe, yet upon transformation to γ-Fe they only shift slightly on the stability map and remain within the nanostructure zone. Additions of Ni and Cr are not expected to stabilize the grain size of α-Fe and remain inside the unstable zone of the stability map (i.e., bulk states), meaning that neither contribute to high-temperature grain size stability. Only in the case of Fe-Au [Fig. 4(d)] does the stable grain size of γ-Fe decrease after the transformation even though the temperature is increased. This trend is found with respect to temperature, as well as with time [Fig. 3(a)], in line with our schematic in Fig. 1.

It should be noted that the results in Fig. 4 for $Fe_{91}Ni_8Zr$ and for two of our alloys ($Fe_{81}Cr_{19}Mg$ and $Fe_{90}B_{10}$) reveal a two-phase coexistence. This was deliberate for $Fe_{91}Ni_8Zr$ as the authors studied the transformation mechanism in those alloys, whereas in our alloys, the two-phase coexistence was transient: the transformation did not complete during the annealing time, yet the peaks of the unstable phase decreased in intensity with time. The effect of the transformation itself on thermal stability is a complex topic, owing to the thermodynamics of segregation to interphase boundaries simultaneously with grain boundaries of both phases, and will be the subject of future work. Here we selected annealing temperatures that were high enough such that transformation completes rapidly, and thermal stability is studied in a single-phase alloy (Figs. 3 and S1).

In our alloy design approach, we intended for the high-temperature thermal stability of γ-Fe in our Fe-Au alloy to stem from thermodynamic stabilization by grain boundary segregation of Au atoms, and the experimental results generally support such an interpretation. Above the transformation temperature, γ-Fe is the only observed phase, meaning that all Au atoms dissolved into it. No stable compounds are known for this system [50], and no oxidation is expected for such alloys [51], so that Au atoms are either in the bulk of Fe grains or along their grain boundaries. Segregation of Au at grain boundaries is well documented in α-Fe [52,53], and even though the fcc structure of γ-Fe differs by its coordination number and grain boundary structure, the main predictor for segregation —a large mismatch in atomic size [54,55]—remains unchanged. Indeed, our estimations of ΔH_{seg} revealed similar values between the phases (see Supplemental Material [24]). Finally, the effects of kinetics on the observed results must be addressed: whether the lower grain size in γ-Fe is the result of much lower mobility or some other hindrance to microstructure evolution. We

estimated the diffusion lengths in our alloy and found them to be significantly larger than the grain size under our annealing conditions. Any impurity effects can be neglected simply because our comparison to other alloys (most prepared and annealed in the same manner) revealed the conventional behavior of larger γ-Fe grains (Fig. 4). Even drag exerted by Au solute in grain boundaries was found to be negligible at the high temperatures and long annealing times employed in this study. The complete details of our kinetic analysis can be found in the Supplemental Material [24].

The counterintuitive behavior exhibited by our nanocrystalline Fe-Au alloy sidesteps the conventional paradigm of grain growth: by combining a recrystallizationlike event (phase transformation) with alloy design criteria for stable nanocrystalline alloys, we attained a lower and stable grain size at a higher temperature. The phase transformation provides a clean slate for the system to find its new equilibrium grain size, which may be lower than the grain size in the preceding low-temperature phase for certain solutes. We demonstrated that this behavior could be cycled several times, and therefore, our approach provides a critical test for theories of thermodynamic stabilization of nanostructures by grain boundary segregation. These are often challenged by the effect of the deformed initial microstructure and by the emergence of second-phase precipitates which contribute to kinetic stabilization [48,49]. Our approach also allows the design of an alloy having some or all of its phases stabilized by different solutes, so that it remains nanocrystalline in a wide temperature range, with a tailored grain size for each phase. Such alloys may exhibit excellent mechanical properties at very high temperatures, possibly superior to their low-temperature properties. Based on the grain growth observed for Fe-Au alone, we expect that the alloy could become significantly stronger as the temperature is increased through the transformation and that the mechanical properties could be switched repeatedly by cycling the temperature around the transformation temperature. We therefore believe that this could present a new approach to high-temperature applications without requiring refractory materials.

This work was supported by the U.S. Army Research Office under Grant No. W911NF-14-1-0539, by the U.S. National Science Foundation under Grant No. DMR-1606914, and by the Marie Skłodowska Curie Global Fellowship under Grant No. 740384. XRD work was performed at the Center for Materials Science and Engineering (CMSE), which is supported by the National Science Foundation under Grant No. DMR-1419807. CMSE is part of the Massachusetts Institute of Technology. FIB and part of the TEM work were performed at the Harvard University Center for Nanoscale Systems (CNS), a member of the National Nanotechnology Coordinated Infrastructure Network (NNCI), which is supported by the National Science Foundation under NSF ECCS Grant No. 1541959. Fruitful discussions with A. R. Kalidindi are gratefully acknowledged.

*Corresponding author.
dor.amram.da@gmail.com

[1] R. D. MacPherson and D. J. Srolovitz, Nature (London) **446**, 1053 (2007).
[2] B. Bayerlein, P. Zaslansky, Y. Dauphin, A. Rack, P. Fratzl, and I. Zlotnikov, Nat. Mater. **13**, 1102 (2014).
[3] A. P. Sutton and R. W. Balluffi, *Interfaces in Crystalline Materials* (Oxford University Press, Oxford, 2006).
[4] P. R. Cantwell, E. A. Holm, M. P. Harmer, and M. J. Hoffmann, Scr. Mater. **103**, 1 (2015).
[5] E. R. Homer, E. A. Holm, S. M. Foiles, and D. L. Olmsted, JOM **66**, 114 (2014).
[6] G. S. Rohrer, Curr. Opin. Solid State Mater. Sci. (2016).
[7] A. Rollett, F. J. Humphreys, G. S. Rohrer, and M. Hatherly, *Recrystallization and Related Annealing Phenomena* (Elsevier, New York, 2004).
[8] R. A. Grange, Metall. Trans. **2**, 65 (1971).
[9] Y. Estrin, G. Gottstein, E. Rabkin, and L. S. Shvindlerman, Scr. Mater. **43**, 141 (2000).
[10] T. Chookajorn, H. A. Murdoch, and C. A. Schuh, Science **337**, 951 (2012).
[11] P. A. Manohar, M. Ferry, and T. Chandra, ISIJ International (1989-) (Iron and Steel Institute of Japan) **38**, 913 (1998).
[12] I.-W. Chen and X.-H. Wang, Nature (London) **404**, 168 (2000).
[13] W. W. Mullins, J. Appl. Phys. **28**, 333 (1957).
[14] C. V. Thompson, Annu. Rev. Mater. Res. **42**, 399 (2012).
[15] D. Amram, L. Klinger, N. Gazit, H. Gluska, and E. Rabkin, Acta Mater. **69**, 386 (2014).
[16] R. Kirchheim, Acta Mater. **50**, 413 (2002).
[17] M. Saber, C. C. Koch, and R. O. Scattergood, Mater. Res. Lett. **3**, 65 (2015).
[18] R. A. Andrievski, J. Mater. Sci. **49**, 1449 (2014).
[19] T. Chookajorn and C. A. Schuh, Phys. Rev. B **89**, 064102 (2014).
[20] J. R. Trelewicz and C. A. Schuh, Phys. Rev. B **79**, 094112 (2009).
[21] A. R. Kalidindi and C. A. Schuh, Comput. Mater. Sci. **118**, 172 (2016).
[22] A. R. Kalidindi and C. A. Schuh, Acta Mater. **132**, 128 (2017).
[23] W. Xing, A. R. Kalidindi, and C. A. Schuh, Scr. Mater. **127**, 136 (2017).
[24] See Supplemental Material at http://link.aps.org/supplemental/10.1103/PhysRevLett.121.145503 for complete details on methods, model derivation, additional results and extended discussion, which includes Refs. [25–44].
[25] H. A. Murdoch and C. A. Schuh, J. Mater. Res. **28**, 2154 (2013).
[26] D. Wolf, Acta Metall. Mater. **38**, 791 (1990).
[27] D. Amram and E. Rabkin, JOM **68**, 1335 (2016).
[28] D. Amram, O. Kovalenko, and E. Rabkin, Acta Mater. **98**, 343 (2015).
[29] C. C. Chou and C. M. Wayman, Mater. Sci. Eng. A **149**, 73 (1991).
[30] D. Amram and E. Rabkin, ACS Nano **8**, 10687 (2014).
[31] C. Langlois, P. Benzo, R. Arenal, M. Benoit, J. Nicolai, N. Combe, A. Ponchet, and M. J. Casanove, Nano Lett. **15**, 5075 (2015).

[32] F. S. Buffington, K. Hirano, and M. Cohen, Acta Metall. **9**, 434 (1961).
[33] A. W. Bowen and G. M. Leak, Metall. Trans. **1**, 1695 (1970).
[34] L. Huang, W. Lin, K. Wang, S. Song, C. Guo, Y. Chen, Y. Li, and F. Liu, Acta Mater. **154**, 56 (2018).
[35] S. Hofmann and J. Erlewein, Scr. Metall. **10**, 857 (1976).
[36] R. J. Borg and D. Y. F. Lai, Acta Metall. **11**, 861 (1963).
[37] D. Wolf, Philos. Mag. A **62**, 447 (1990).
[38] G. V. Raynor and V. G. Rivlin, Bull. Alloy Phase Diagrams **2**, 102 (1981).
[39] *ASM Handbook Volume 3: Alloy Phase Diagrams*, edited by H. Baker (American Soc. for Metals, Metals Park, OH, 1992).
[40] A. A. Nayeb-Hashemi, J. B. Clark, and L. J. Swartzendruber, Bull. Alloy Phase Diagrams **6**, 235 (1985).
[41] M. Jiang, K. Oikawa, T. Ikeshoji, L. Wulff, and K. Ishida, J. Phase Equilib. **22**, 406 (2001).
[42] S. Hertzman and B. Sundman, CALPHAD: Comput. Coupling Phase Diagrams Thermochem. **6**, 67 (1982).
[43] P. Lejček, S. Hofmann, and J. Janovec, Mater. Sci. Eng. A **462**, 76 (2007).
[44] D. Favez, J. D. Wagnière, and M. Rappaz, Acta Mater. **58**, 1016 (2010).
[45] H. Kotan, K. A. Darling, M. Saber, R. O. Scattergood, and C. C. Koch, J. Mater. Sci. **48**, 2251 (2013).
[46] L. Huang, W. Lin, B. Lin, and F. Liu, Acta Mater. **118**, 306 (2016).
[47] H. Kotan and K. A. Darling, Mater. Charact. **138**, 186 (2018).
[48] D. Amram and C. A. Schuh, Acta Mater. **144**, 447 (2018).
[49] W. Xu, L. Li, M. Saber, C. C. Koch, Y. Zhu, and R. O. Scattergood, Metall. Mater. Trans. A **46**, 4394 (2015).
[50] H. Okamoto, T. B. Massalski, L. J. Swartzendruber, and P. A. Beck, Bull. Alloy Phase Diagrams **5**, 592 (1984).
[51] D. Amram, L. Klinger, and E. Rabkin, Acta Mater. **61**, 5130 (2013).
[52] C. Zamponi, U. Schürmann, T. Jurgeleit, L. Kienle, and E. Quandt, Int. J. Mater. Res. **106**, 103 (2015).
[53] D. Amram, Y. Amouyal, and E. Rabkin, Acta Mater. **102**, 342 (2016).
[54] P. Lejček, *Grain Boundary Segregation in Metals* (Springer, Berlin, 2010).
[55] P. Wynblatt and R. C. Ku, Surf. Sci. **65**, 511 (1977).